Ultra-low Chirp PCF Mach-Zehnder Interferometer

William O. F. Carvalho[1,*], Danilo H. Spadoti[2], Enrique Silvestre[3], and Felipe Beltran-Mejia[1]

[1] *National Institute of Telecommunications – INATEL, Av. Joao Camargo 510, Santa Rita do Sapucai, 37540-000, Brazil*
[2] *Federal University of Itajuba, Av. BPS 1303, Itajuba, 37500-903, Brazil*
[3] *Department of Optics, ICMUV, University of Valencia, 46100 Burjassot, Valencia, Spain*
**Corresponding author: williamofcarvalho@gmail.com*

Received XX Month XXXX; revised XX Month, XXXX; accepted XX Month XXXX; posted XX Month XXXX (Doc. ID XXXXX); published XX Month XXXX

A Photonic Crystal Fiber Mach-Zehnder Interferometer design was optimized to obtain high performance and ultra-low chirp. Two Long Period Gratings were used to excite the cladding modes, and the rich structure of the cladding was tailored to obtain a slightly chirped Free Spectral Range, as required by the ITU-T Norm G.694.1. Finally, a fabrication tolerance analysis was performed. The advantages of the proposed device are an ultra-low chirp, high bandwidth and fabrication robustness tolerance.

OCIS codes: (230.1150) All-optical devices; (060.2280) Fiber design and fabrication; (060.5295) Photonic crystal fibers.

http://dx.doi.org/10.1364/AO.99.099999

1. INTRODUCTION

All-fiber Mach-Zehnder Interferometers (MZI) have been extensively used and studied to create passive optical devices [1–3]. In optical communications, MZIs can be used in electro-optic modulators, Dense Wavelength Division Multiplexing (DWDM) filters and all-optical (de)multiplexer [4–6]. In other areas, MZIs are also used in sensing applications as transducers for measuring temperature [7], strain, external refractive index and curvature [8].

An all-fiber MZI can be constructed by two Long-Period Gratings (LPG) written in series in a single fiber. These create two different paths that act as the arms of the interferometer as shown by the arrows in Fig. 1(a). An LPG is a periodic perturbation of the core's refractive index, in such a way that high order cladding modes are excited. These modes leave a spectral gap in the core, known as stop bands [9]. Hence, the parameters of both LPGs are designed to reach the match condition in the desired wavelength. When two identical LPGs are written in series, part of the energy of the higher order modes is recoupled inside the core. In this way, light propagates at the same time through the core and through the cladding. The difference between the two optical paths creates an interference pattern as shown in Fig. 1(b). And controlling the Free Spectral Range (FSR)—the distance between these peaks—is crucial for the (de)multiplexing process [2,10]. Usually, FSR is not constant but a function of the wavelength, that is, FSR is chirped because the standard fiber's models are not designed for these purposes.

Here, we report a Photonic Crystal Fiber (PCF) optimized to obtain different FSR profiles, such as the one required by the ITU-T norm G.694.1 [11]. On the other hand, and as a proof of concept, a PCF optimization was made to obtain an ultra-low chirp MZI, resulting in a constant FSR for the entire C band. A PCF is a microstructured fiber made with pure silica with an array of air-holes equally spaced that extends along the longitudinal axis forming the cladding region. A defect on the array, for example, the absence of an air-hole at the center of the fiber, defines the core as shown in the inset of Fig. 1(b). The high difference of the refractive index between silica and air, along with the forbidden broadband propagation across the microstructured region, confines the light inside the core [12,13]. In previous studies, the sensing arm is formed by including a second defect inside the micro-structure as done by Liang et al. [7]. Here, in our simulations, we have reduced the size of the innermost air-holes in order to use it as a sub-cladding and, at the same time, exploit its geometrical richness to tailor the cladding's mode dispersive properties.

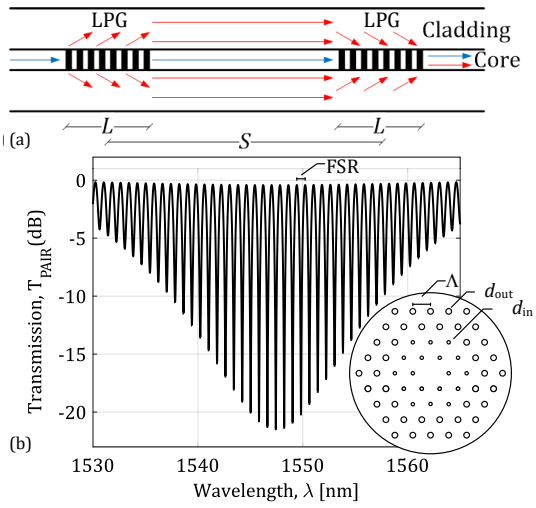

Fig. 1 (a) Schematic of a PCF-MZI configuration to obtain (b) an interference pattern. The separation between LPGs modify the optical path difference, in such a way there is a constructive/destructive interference. Inset shows the cross-section of a PCF with a pitch Λ and two different hole diameters for the inner and outer claddings, d_{in} and d_{out} respectively.

In this paper we present PCF configurations that effectively tunes the dispersion in order to tailor the interferometric pattern of the MZI. This paper is structured in three sections: the following section describes the LPG spectral characteristics as well as the MZI behavior and its FSR features. The next one presents the optimization results of two PCF designs and the expected effect of the fabrication tolerances. Finally, we discuss our results and the future perspectives.

2. THEORY

The LPG parameters were calculated using the Coupled-Mode Theory [14] to obtain the spectral band gaps. The excitation of the higher order modes occurs when there is a phase match between the fundamental mode and the cladding modes. This match is given by the Floquet condition,

$$\beta_{co} - \beta_{cl}^{(i)} = K, \tag{1}$$

where β_{co} and $\beta_{cl}^{(i)}$ are the propagation constants of the fundamental mode and the ith cladding mode, respectively, $K = 2\pi/\Lambda_{LPG}$ and Λ_{LPG} is the grating period [15].

The stop bands appear at the minima of the LPG transfer function [9],

$$T_{LPG} = 1 - \kappa\kappa^* \left[\frac{\sin(sL)}{s}\right]^2, \tag{2}$$

where κ is the coupling coefficient and κ^* is its conjugate, L is the grating length, $s = [\kappa\kappa^* + (\Delta\beta/2)^2]^{1/2}$ and $\Delta\beta = \beta_{co} - \beta_{cl}^{(i)} - K$ is the detuning in the propagation constant, which is zero for a perfect match between modes. The grating strength κL is chosen as $\pi/4$ to direct half of the power to the cladding mode [14].

As shown in Fig. 1(a), if there is a second identical LPG separated by a distance S, the cladding modes are coupled again to the core. This creates an interferometric pattern in the stop band with a sinusoidal behavior [9],

$$T_{PAIR} = (T_{LPG})^2 + (\alpha R_{LPG})^2 - 2\alpha T_{LPG} R_{LPG} \cos(\Psi), \tag{3}$$

where $\Psi = (\beta_{co} - \beta_{cl})(S + L)$ is the relative phase between modes, $R_{LPG} = 1 - T_{LPG}$ and α is the attenuation coming by the cladding mode radiation losses. Notice that the transfer function of a pair of LPGs is the sum of the transfer function of each LPG with the transfer function of the light that returns to the core, as shown by the first two terms in (3). The third term represents an interaction between these modes, occurring interference.

Furthermore, each interferometer peak occurs when the relative phase between modes is a multiple of 2π. Thus, the Free Spectral Range can be described as the ratio between 2π and the derivative of Ψ with respect to the wavelength λ, becoming:

$$\mathrm{FSR} = \frac{2\pi}{\frac{d\Psi}{d\lambda}} \tag{4}$$

To obtain the required chirp profile, we used the Nelder-Mead method as in [12]. This adaptation uses a semi-analytic function to simulate the effect of scale on a dispersive structure, allowing to accelerate the Nelder-Mead method convergence and to avoid stagnation. As a first approach, we neglected any LPG fabrication errors and considered uniform gratings perpendicular to the longitudinal axis of the fiber, in order to simplify the optimization process. In consequence, these LPGs will only couple axially symmetric modes LP_{0n} [16]. Moreover, for the analysis herein, only the first two lower order modes were used for the coupled mode analysis as they achieve higher modal amplitudes [17].

In the following section, we show our results for two different optimization objectives: a PCF that minimizes the chirp and meets the ITU-T norm; and a PCF that cancels – to a great extent – the chirp effects in the MZI. The parameters used during the optimization processes are the geometrical features of the PCFs depicted in Figs. 1 and 2, that is, the pitch Λ and the diameter of the inner and outer holes d_{in} and d_{out}, respectively.

3. RESULTS

For the first objective, the merit function was given by $|\mathrm{FSR} - \mathrm{FSR}_{ITU}|^2$, where FSR_{ITU} is the FSR required for adjacent DWDM carriers [11]. Likewise, a slightly similar merit function was used to optimize the PCF's parameters for an ultra-low chirp MZI. In this case, the merit function was given by $|\mathrm{FSR} - 0.8\,\mathrm{nm}|^2$, where a constant fringe spacing 0.8 nm value was chosen to compare the 100 GHz FSR in DWDM channels. These optimizations were performed in a computer with an Intel i5-3317 processor of 1.7 GHz and 4 GB RAM. We also used Comsol for the Finite Element modal analysis of the PCF and Matlab to control the optimization process and the post-processing analysis.

A. PCF with MZI slightly chirped

The parameters of the first optimized PCF design have been adjusted to maintain FSR constant in frequency as the spacing between DWDM carriers in the ITU-T norm (100, 50, 25, 12.5 GHz). In the wavelength domain, FSR is slightly chirped, then the optimization process approximates the FSR curves (dashed line) with the ITU-T norm (solid line), as it is shown in Fig. 2. This optimization lasted about four hours and forty minutes and reached the PCF parameters after 82 iterations. In fact, this PCF design matches the slope of any ITU-T DWDM channels spacing, by only changing the LPGs' pair separation S. The results of this optimization are summarized in Table 1.

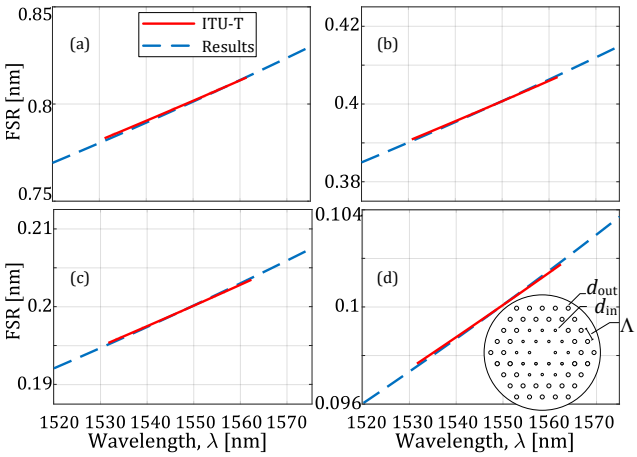

Fig. 1. The slightly chirped FSR and the optimized PCF geometry. The PCF parameters have been adjusted to match the FSR-MZI (blue dashed line) almost equal to the FSR of the ITU-T norm (red solid line). The PCF produced MZIs with FSR of (a) 100, (b) 50, (c) 25 and (d) 12.5 GHz.

Table 1 Parameters for the optimized Mach-Zehnder Interferometer.

FSR	Separation S [m]	LPG Length L [mm]	LPG Period Λ [μm]	PCF Parameters [μm]
100 GHz 50 GHz 25 GHz 12.5 GHz	0.590 1.188 2.383 4.775	8.077	149.580	din = 0.44 dout = 0.74 Λ = 2.33
Constant in 0.8 nm	0.172	8.031	78.736	din = 0.43 dout = 1.00 Λ = 1.84

B. PCF with Ultra-low chirp MZI

As a proof of principle, an MZI with a constant FSR was designed. For this reason, the second optimized PCF design had its geometrical parameters adjusted to maintain FSR constant in all C band. As explained above, the merit function levels the FSR curve to a constant equal to 0.8 nm, as it is shown in Fig. 3. This optimization lasted about five hours and twenty minutes after 93 iterations.

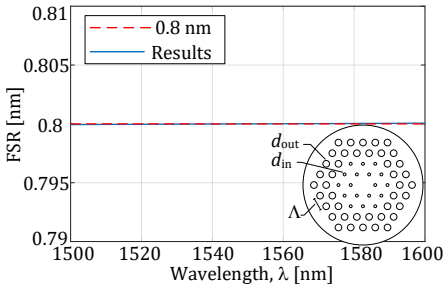

Fig. 2. A nearly-constant FSR with an ultra-low chirp for an optimized PCF geometry. A constant target of 0.8 nm was chosen (red dashed line) to match FSR-MZI (solid blue line) with a constant spacing value.

This PCF design keeps the FSR constant in all C band. Moreover, the FSR remains constant for any value of S in all C band. The parameters of the optimized MZI geometry are listed on the last row of Table 1.

C. Fabrication Tolerance

The fabrication of micro-structured fibers requires high precision techniques. This becomes even more critical when cladding modes are used, since light is going to propagate around the air-holes. For this reason, it is important to know beforehand the fabrication error tolerance of the structure. Combining the parameters variation (d_{in} , d_{out} and Λ) in a deviation of ± 5 %, it obtains different FSR values as expected. For this purpose, we used variations of ± 5 % that occurred realistically according the fiber fabrication process as explained in [12]. Therefore, the parameters enlargement and contraction has been adjusted to keep d_{in}/Λ and d_{out}/Λ constant. The results are shown in Fig. 4 for both MZI designs. In both plots, the dashed red lines represent the worst cases while the blue solid lines represent the proposed geometries as shown in Fig. 2 and Fig. 3.

In both cases, the contraction of 5 % resulted in a smaller slope of the FSR, while the enlargement of 5 % resulted in a larger slope of the FSR. Note in Fig. 4 (a) FSR has a maximum deviation of ± 0.004 nm, while in Fig. 4 (b) the maximum deviation of FSR is ± 0.0013 nm. These deviations were calculated by subtracting the values between the precise PCF and the worst case on the edges of the C band (1530 and 1565 nm).

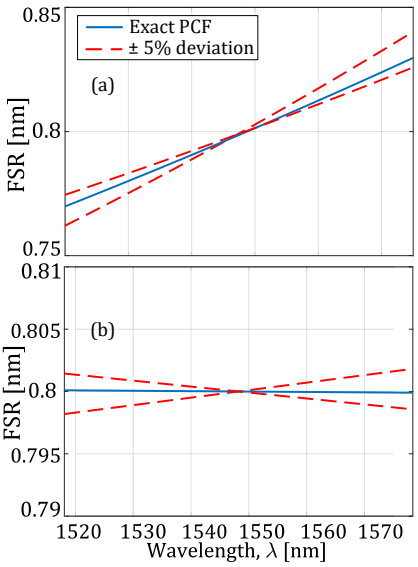

Fig. 3. Comparison of the FSR for MZIs with the optimized geometry (solid blue line) and for the worst cases (red dashed line) considering 5% of inaccuracies in the fabrication of the PCFs. (a) slightly chirped PCF-MZI optimized for the ITU-T norm and (b) PCF-MZI with ultra-low chirp.

4. CONCLUSIONS

We present an optimized PCF design that precisely tailors the FSR of a Mach-Zehnder interferometer. The precise management of the dispersion of the cladding modes, ensures the correct slightly chirped FSR according to the ITU-T norm. Moreover, the parameters of the first row in Table 1 show that the same PCF geometry and the same pair of LPGs fulfils the FSR requirements of the ITU-T norm. In addition, the FSR is almost inversely proportional to S. In the same way, another optimized PCF design was shown to obtain an ultra-low chirp MZI that maintains FSR constant in the C band.

Moreover, the structures presented here show a good tolerance to fabrication errors. A small impact on the FSR was observed for fabrication tolerances of up to 5 %. Thereby, these deviations may not introduce considerable errors in communications devices.

Summing up, we have presented two optimized PCF structures that precisely tailor the FSR of a single Mach-Zehnder Interferometer. These devices have shown to be highly accurate and robust to fabrication errors. For this reason, these all-PCF MZIs can be used in many passive optical devices, once they maintain the chirp in optical communications systems, ensuring reliability and information safety, avoiding cross-talk between adjacent channels and carriers' deviations.

References

1. Y. Cao, H. Liu, Z. Tong, S. Yuan, and J. Su, "Simultaneous measurement of temperature and refractive index based on a Mach-Zehnder interferometer cascaded with a fiber Bragg grating," Opt. Commun. **342**, 180–183 (2015).
2. F. Horst, W. M. Green, S. Assefa, S. M. Shank, Y. A. Vlasov, and B. J. Offrein, "Cascaded Mach-Zehnder wavelength filters in silicon photonics for low loss and flat pass-band WDM (de-) multiplexing," Opt. Express **21**, 11652–11658 (2013).
3. P. Chen, X. Shu, and K. Sugden, "Ultra-compact all-in-fiber-core Mach-Zehnder interferometer," Opt. Lett. **42**, 4059–4062 (2017).
4. R. Palmer, L. Alloatti, D. Korn, P. C. Schindler, M. Baier, J. Bolten, T. Wahlbrink, M. Waldow, R. Dinu, W. Freude, C. Koos, and J. Leuthold, "Low Power Mach-Zehnder Modulator in Silicon-Organic Hybrid

Technology," IEEE Photonics Technol. Lett. **25**, 1226–1229 (2013).
5. A. P. Ovvyan, N. Gruhler, S. Ferrari, and W. H. P. Pernice, "Cascaded Mach–Zehnder interferometer tunable filters," J. Opt. **18**, 64011 (2016).
6. C. Li, T. Ning, C. Zhang, J. Li, C. Zhang, X. Wen, H. Lin, and L. Pei, "All-fiber multipath Mach-Zehnder interferometer based on a four-core fiber for sensing applications," Sensors Actuators A Phys. **248**, 148–154 (2016).
7. H. Liang, W. Zhang, H. Wang, P. Geng, S. Zhang, S. Gao, C. Yang, and J. Li, "Fiber in-line Mach Zehnder interferometer based on near-elliptical core photonic crystal fiber for temperature and strain sensing," Opt. Lett. **38**, 4019–4022 (2013).
8. S. Zhang, H. Gong, Z. Qian, Y. Jin, and X. Dong, "Fiber curvature sensor based on Mach–Zehnder interferometer using up-taper cascaded long-period grating," Microw. Opt. Technol. Lett. **58**, 246–248 (2016).
9. B. H. Lee and J. Nishii, "Dependence of fringe spacing on the grating separation in a long-period fiber grating pair.," Appl. Opt. **38**, 3450–3459 (1999).
10. J. Yao, "Microwave photonics," Conf. Proc. - Int. Conf. Indium Phosphide Relat. Mater. **27**, 212–214 (2012).
11. ITU-T, *Spectral Grids for WDM Applications: DWDM Frequency Grid* (2012), p. 16.
12. F. Beltrán-Mejía, C. M. B. Cordeiro, P. Andrés, and E. Silvestre, "Broadband dispersion compensation using inner cladding modes in photonic crystal fibers," Opt. Express **20**, 3467 (2012).
13. W. Jin, J. Ju, H. L. Ho, Y. L. Hoo, and A. Zhang, "Photonic crystal fibers, devices, and applications," Front. Optoelectron. **6**, 3–24 (2013).
14. V. Bhatia, "Properties and sensing applications of long-period gratings," Ph.D. Dissertation, Virginia Tech, Blacksburg (1996).
15. V. L. Iezzi, J.-S. Boisvert, S. Loranger, and R. Kashyap, "3D printed long period gratings for optical fibers," Opt. Lett. **41**, 1865–1868 (2016).
16. S. M. Tripathi, A. Kumar, R. K. Varshney, Y. B. P. Kumar, E. Marin, and J.-P. Meunier, "Strain and Temperature Sensing Characteristics of Single-Mode–Multimode–Single-Mode Structures," J. Light. Technol. **27**, 2348–2356 (2009).
17. F. Beltrán-Mejía, C. R. Biazoli, and C. M. B. Cordeiro, "Tapered GRIN fiber microsensor," Opt. Express **22**, 30432–30441 (2014).

Funding Information. Finep/Funttel (01.14.0231.00) under the Radiocommunication Reference Center – CRR, project of the National Institute of Telecommunications – Inatel, Brazil.